Learning to Assist Bimanual Teleoperation using Interval Type-2 Polynomial Fuzzy Inference

Ziwei Wang, *Member, IEEE,* Haolin Fei, Yanpei Huang, *Member, IEEE,* Quentin Rouxel, Bo Xiao, *Member, IEEE,* Zhibin Li, *Member, IEEE,* and Etienne Burdet, *Member, IEEE*

***Abstract*—Assisting humans in collaborative tasks is a promising application for robots, however effective assistance remains challenging. In this paper, we propose a method for providing intuitive robotic assistance based on learning from human natural limb coordination. To encode coupling between multiple-limb motions, we use a novel interval type-2 (IT2) polynomial fuzzy inference for modeling trajectory adaptation. The associated polynomial coefficients are estimated using a modified recursive least-square with a dynamic forgetting factor. We propose to employ a Gaussian process to produce robust human motion predictions, and thus address the uncertainty and measurement noise of the system caused by interactive environments. Experimental results on two types of interaction tasks demonstrate the effectiveness of this approach, which achieves high accuracy in predicting assistive limb motion and enables humans to perform bimanual tasks using only one limb.**

***Index Terms*—Human-robot collaboration, Bimanual manipulation, IT2 polynomial fuzzy system, Robot learning, Gaussian process.**

I. Introduction

ROBOTS can assist humans and potentially alleviate their workload during collaborative tasks, while the human user typically contributes to the adaptation of trajectories and efforts. Effective human-robot coordination is crucial to ensure that the interaction is transparent to the user. A supervised teleoperation scheme can allow the robot to follow human commands [1]–[3]. Similarly, the robotic agent of [4] assists in trajectory training for novices based on task-dependent reinforcement learning. From a cognitive perspective, robots could be made more flexible and better interact with human users by learning from human movements humans using logical inference. Recent works have emphasized the importance of the robot to generate commands based on the prediction of the user's movements [5]–[7]. Different from transfer learning [8]–[10], learning from demonstration [11]–[14] or human posture prediction in physical human-robot interaction [15], our idea is to generate human-robot assistive control based on the coordination observed in bimanual control or in the collaborative control between multiple humans.

Intrinsic nonlinearity and uncertainty of human motion pose great challenges to developing the aforementioned coordination models. Transferring cognitive processes observed in human brain to robotic applications may be used to generate behaviours that are robust to changes in the environment [16]. Different from neural networks [17] and regression models [18] that rely on an arbitrary system structure, fuzzy systems can represent nonlinear plants starting from human know-how, which can reduce the computational complexity and the number of required parameters [19]. Takagi-Sugeno fuzzy model based (T-S FMB) systems realize nonlinear approximation capability with arbitrary accuracy through a weighted sum of linear subsystems [20]. As an effective extension, the polynomial fuzzy model relaxes the restrictions on the argument domain, allows the system matrices to contain polynomials, and therefore can express nonlinearties well [21]. In terms of T-S and polynomial FMB (PFMB) identification, most reported methods obtain fuzzy sets and fuzzy rules by clustering methods and perform linear identification operations with least-square-like under each rule [22], [23]. The above algorithms leveraged the first order of input data and inter-data relationship, i.e. the input data are decoupled. However, the limb motion in each dimension contributes to the other in a coupled way, thus the above approaches might miss the intra-data relationship.

Moreover, they are not designed to deal with parameter uncertainty in the membership function induced by human motion, where measurement errors may result in vibrations in the membership function and thereby degrade the modeling accuracy. The interval type-2 (IT2) fuzzy set is a promising tool to handle such uncertainties, captured within the footprint of uncertainty (FOU) formed by the upper and lower membership functions (i.e., UMF and LMF). In [24], [25], the UMF and LMF are constructed by adjusting the fuzzy partition matrix exponent in terms of fuzzy c-means (FCM) clustering, which is beneficial to address parameter uncertainty in system identification. The FOU is obtained through the heuristic-based and histogram-based methods by scaling the parameters in predefined type-1 membership functions [26]. However, the above methods for constructing IT2 fuzzy sets can only handle the parameter uncertainty within a predefined range, which

This work was partly supported by the UK EPSRC program grant FAIR-SPACE EP/R026092/1 and by the European Commission grants H2020 PH-CODING (FETOPEN 829186) and NIMA (FETOPEN 899626). (*Corresponding author: Ziwei Wang and Yanpei Huang*)

Ziwei Wang, Yanpei Huang, and Etienne Burdet are with the Department of Bioengineering, Imperial College London, W12 0BZ, United Kingdom. Ziwei Wang is also with the School of Engineering, Lancaster University, LA1 4YW, United Kingdom (e-mail: z.wang82@lancaster.ac.uk, yanpei.huang@imperial.ac.uk).

Haolin Fei is with the School of Engineering, Lancaster University, LA1 4YW, United Kingdom.

Quentin Rouxel was with the Edinburgh Centre for Robotics, University of Edinburgh, United Kingdom. He is now with the Inria Nancy - Grand Est, Université de Lorraine, CNRS, 54600 Villers-lès-Nancy, France.

Bo Xiao is with the Hamlyn Centre for Robotic Surgery, Imperial College London, London, SW7 2AZ, United Kingdom.

Zhibin Li is with the Department of Computer Science, University College London, London, United Kingdom.

relies on the prior knowledge of system uncertainty.

To address the intrinsic nonlinearity and uncertainty of human motion for human-robot coordination, this paper introduces a Gaussian process (GP) based IT2 polynomial fuzzy learning (GP-IT2PFL) algorithm, which enables humans to perform the bimanual task only by one limb. The proposed method aims to attain a trajectory-level shared control in teleoperation by utilizing a learned policy that is anticipated by the human operator. Based on the modified FCM clustering with z-score normalization, the entire task is classified into fuzzy sets yielding corresponding membership functions. Mapping nonlinearity, parameter uncertainty, and measurement noise can be handled effectively, where the FOU is constructed by a Gaussian process. The innovations of the GP-IT2PFL algorithm are as follows:

(1) *Cross-polynomial* and *solo-polynomial matrices* are introduced to reflect the intrinsic coupling of input data with different features and dimensions, enabling to represent the intra- and inter-class features in human limbs coordination.

(2) The UMF and LMF are developed by the posterior distribution predicted through a non-parametric Gaussian process, which facilitates the capture of parameter perturbations due to measurement noise and system uncertainty. Therefore, the GP-IT2PFL algorithm is featured by data-driven and does not depend on the identification structure.

The paper first describes an IT2 polynomial fuzzy learning method with Gaussian process based membership function, which aims at generating human-robot assistive control. Then we tested the GP-IT2PFL algorithm in two human-robot collaboration scenarios. First, a foot-robot coordination experiment was carried out for grasping, picking and placing tasks. We recorded hand-foot coordination while performing these tasks. The GP-IT2PFL algorithm then was used to generate hand-like trajectories for foot-robot coordination to assist foot behaviors thus freeing up the hands for direct manipulation. Second, we recorded the movements of two collaborating humans in a human-robot shared telesurgery experiment, then modeled one human as a robot partner, where the robot trajectory was generated by the GP-IT2PFL algorithm that assisted humans in a peg-transfer task. These applications validate the developed algorithms and illustrate some of the opportunities they open.

II. Methods

A. Mathematical Notation

$\mathbb{Z}^+[a,b]$ refers to the set of natural numbers from a to b. For $x = [x_1, x_2, \ldots, x_n] \in \mathbb{R}^n$ and $d \in \mathbb{Z}^+[1,+\infty]$, $G_d(x_1) = [x_1^{d-1}, x_1^{d-2}, \ldots, 1]^{\mathrm{T}}$ and $\mathcal{G}_d(x) = [G_d(x_1), G_d(x_2), \ldots, G_d(x_n)] \in \mathbb{R}^{d\times n}$. $\mathrm{col}_{i=1}^n\{x_i\} \in \mathbb{R}^n$ is the column vector whose x_i is the ith entry. $\mathcal{V}_d(x) \in \mathbb{R}^{n\times d}$ denotes the Vandermonde matrix of degree $d-1$. "$\circ$" is the Hadamard product. For $y = [y_1, y_2, \ldots, y_n] \in \mathbb{R}^n$, $\mathcal{P}_{xy} = \sum_{i=1}^n \mathcal{V}_d(x)\mathcal{G}_d(y_i) \in \mathbb{R}^n$ is defined as *cross-polynomial matrix* of a binary tuple x-y. $\mathcal{P}_x = \sum_{i=1}^n \mathcal{V}_d^*(x)\mathcal{G}_d(x_i) \in \mathbb{R}^n$ is the *solo-polynomial matrix* of x, in which $\mathcal{V}_d^*(x)$ is the Vandemonde matrix with all elements of row i being 1. "$\vee$" is the product operator for *cross-polynomial matrix* $\mathcal{P}_{xy}$ and block matrix M such that $M \vee \mathcal{P}_{xy} = \sum_{i=1}^n M_i \circ \mathcal{V}_d(x)\mathcal{G}_d(y_i) \in \mathbb{R}^n$, where M_i is the ith block entry of M. I is the identity matrix of the appropriate dimension.

B. Working Principle

In order to provide trajectory adaptation tailored to a human operator, we construct a unified IT2 polynomial fuzzy framework by utilizing kinesthetic data (i.e., the respective position and velocity) from two-limb coordination. This framework is developed through four steps: (i) Firstly, we utilize an FCM clustering approach to carry out task segmentation, whereby each cluster denotes a distinct subtask; (ii) The resulting membership functions are generated through a Gaussian process, although they are dependent on kinesthetic data and subject to uncertainty arising from human motion; (iii) IT2 polynomial fuzzy model parameters with respect to each subtask are identified online by introducing cross-polynomial and solo-polynomial matrices; and (iv) The adaptation trajectory is produced through the integration of the membership grades and the corresponding fuzzy model. Fig. 1 illustrates how the GP-IT2PFL based inference engine can generate motion adaptation for hand-foot coordination.

Remark 1: The GP-IT2PFL framework can be used to learn human-robot collaboration from various types of multi-limb coordination. In the hand-foot coordination experiment of Section III the coordinated left-hand motion is learned to later automatically accompany the foot motion. In the experiment of Section IV, the two interfaces are controlled by two humans who collaborate on a shared task. During the training phase, the left-hand and foot motion commands are used to generate hand motion commands of the two individuals. In the testing phase, one robot is autonomously controlled by the GP-IT2PFL algorithm to assist the movement of one human's arm. This is validated in the shared telesurgery experiment.

C. Algorithm Implementation

Denote the two-limb motion states at the training stage as $[x_i, y_i]_{i=1}^N$, where the subscript i stands for the ith sample and N the number of samples. It is noticed that the bimanual task usually consists of multiple segments, where the coordination of the two-limb trajectories in each segment is difficult to describe with the same model. Therefore, we utilize the FCM clustering method to perform task segmentation. Since the potential multiple features are contained in $[x_i]_{i=1}^N$, FCM clustering [27] is modified to solve the following optimization problem using z-score normalization

$$\min_{C} \quad \sum_{i=1}^{N}\sum_{j=1}^{l} (\omega_j(x_i))^{\chi} \left\| \frac{x_i - \mu_x}{\sigma_x} - c_j \right\|^2 \tag{1}$$

$$\text{subject to} \quad \sum_{j=1}^{l} \omega_j(x_i) = 1 \tag{2}$$

where l is the number of fuzzy rules extracted by subtractive clustering [28]. μ_x and σ_x are the mean and standard deviation corresponding to $[x_i]_{i=1}^N$, respectively. $\chi > 1$ is the fuzzy

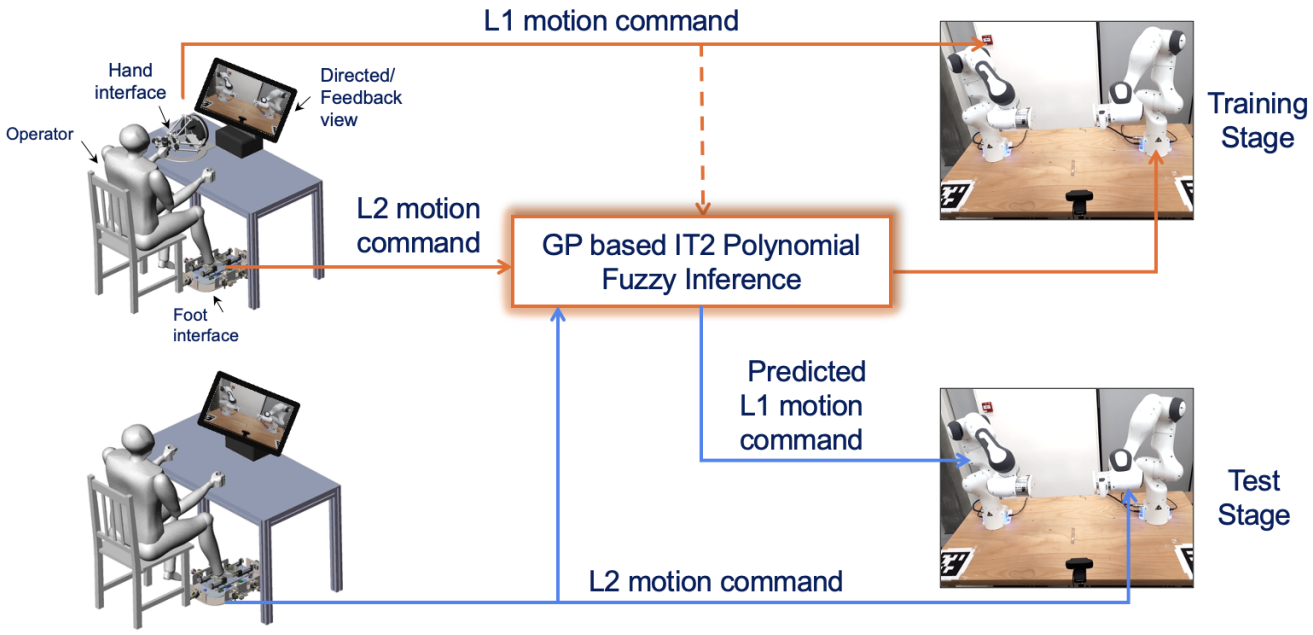

Fig. 1. Diagram of GP-IT2PFL algorithm in two-limb coordination scenario. L1 and L2 refer to two natural limbs, with the left hand and foot serving as illustrative examples. Coordination features between two-limb (i.e., L1 and L2) motions are modeled using natural limb coordination data in the training phase. The resulting model will generate limb-like robot behavior (predicted L1 motion) to assist a human operator.

partition matrix exponent. $C = \{c_1, \ldots, c_l\}$ stands for the set of fuzzy set centers. The membership function with respect to the rule j is denoted by $\omega_j(x_i)$. Taking the Lagrange multiplier $\lambda \in \mathbb{R}_+$ into the optimization problem (1), one can obtain

$$\mathcal{L} = \sum_{i=1}^{N}\sum_{j=1}^{l}(\omega_j(x_i))^{\chi}\left\|\frac{x_i-\mu_x}{\sigma_x} - c_j\right\|^2 + \lambda(1-\sum_{j=1}^{l}\omega_j(x_i)). \tag{3}$$

First-order partial derivatives with respect to λ and $\omega_j(x_i)$ are given by

$$\nabla_{\lambda,\omega_j(x_i)}\mathcal{L} = 0 \Leftrightarrow \begin{cases} \chi(\omega_j(x_i))^{\chi-1}\left\|\frac{x_i-\mu_x}{\sigma_x} - c_j\right\|^2 = \lambda, \\ \sum_{j=1}^{l}\omega_j(x_i) = 1. \end{cases} \tag{4}$$

Solving the above equation group yields the center of each fuzzy set as:

$$c_j = \frac{\sum_{i=1}^{N}(\omega_j(x_i))^{\chi}(x_i-\mu_x)}{\sigma_x\sum_{i=1}^{N}(\omega_j(x_i))^{\chi}}, \tag{5}$$

and

$$\omega_j(x_i) = \begin{cases} 0 & \text{if } x_i = \mu_x + \sigma_x c_k \\ \dfrac{1}{\sum_{k=1}^{l}\left(\frac{\left\|\frac{x_i-\mu_x}{\sigma_x} - c_j\right\|}{\left\|\frac{x_i-\mu_x}{\sigma_x} - c_k\right\|}\right)^{\frac{2}{\chi-1}}} & \text{if } x_i \neq \mu_x + \sigma_x c_k \\ 1 & \text{if } x_i = \mu_x + \sigma_x c_j \end{cases} \tag{6}$$

With the obtained fuzzy clusters (5) and the membership functions (6), the inherent relationship between the hand-foot coordination trajectories can be represented by the following discrete-time polynomial fuzzy system for $j \in \mathbb{Z}^+[1, l]$

$$\begin{aligned} &\text{Rule } j: \text{IF } \mathcal{A}_j(z_i) \text{ is } \mathcal{B}_j \\ &\qquad \text{THEN } y_i = M_j \vee \mathcal{P}_{z_i a_i} + C_j \vee \mathcal{P}_{z_i v_i} + K_j \vee \mathcal{P}_{z_i} \end{aligned} \tag{7}$$

where $z_i = x_i - \mu_x/\sigma_x$ is the z-score normalized form of x_i. $a_i = v_{i+1} - v_i/\Delta T$, v_i and v_{i+1} represent the time-derivative of z_i at ith and $(i+1)$th sample, which can be obtained through Unscented Kalman filter (UKF) to overcome the high computational effort associated with the linearisation of complex motion models. ΔT is the sample time, $\mathcal{A}_j(z_i)$ the premise variable, and $\mathcal{B}_j$ the jth fuzzy set whose centre is c_j. M_j, C_j, and K_j are the coefficient matrices of appropriate dimensions, respectively. $\mathcal{P}_{z_i a_i}$ and $\mathcal{P}_{z_i v_i}$ are the *cross-polynomial system matrices* of $\{z_i, a_i\}$ and $\{z_i, v_i\}$, in which the degree of polynomial matrices is $d_j - 1$. $\mathcal{P}_{z_i} \in \mathbb{R}^n$ is the *solo-polynomial matrix* of z_i.

Remark 2: Introducing the Vandermond matrix in *cross-polynomial* and *solo-polynomial* system matrices enables (7) to incorporate the contributions of each element within a single input (z_i) and of the individual elements of binary input ($\{z_i, a_i\}$ and $\{z_i, v_i\}$). Thus, *solo-polynomial* and *cross-polynomial* system matrices facilitate the representation of intra-class and inter-class relationships of $[x_i]_{i=1}^N$, respectively, exhibiting the intrinsic coupling of limb motion in terms of features and dimensions.

Given $a_i = \text{col}_{p=1}^n\{a_{ip}\} \in \mathbb{R}^n$ and $z_i = \text{col}_{p=1}^n\{z_{ip}\} \in \mathbb{R}^n$ for $p \in \mathbb{Z}^+[1, n]$, we have a more general form of (7) using the equivalent property of polynomial matrix

$$y_i^j = \mathcal{M}_j\langle z_i, a_i\rangle + \mathcal{C}_j\langle z_i, v_i\rangle + \mathcal{K}_j\langle z_i, z_i\rangle, \tag{8}$$

where the *polynomial operator* $\langle z_i, \alpha_i \rangle$ for binary tuple with different features is defined as: $\langle z_i, \alpha_i \rangle = \text{col}_{p=1}^{n}\{\langle z_i, \alpha_{ip} \rangle\}$ with

$$\langle z_i, \alpha_{ip} \rangle = \begin{bmatrix} \sum_{q=1}^{d_j} z_{i1}^{d_j-q} \alpha_{ip}^{q-1} \\ \sum_{q=1}^{d_j} z_{i2}^{d_j-q} \alpha_{ip}^{q-1} \\ \vdots \\ \sum_{q=1}^{d_j} z_{in}^{d_j-q} \alpha_{ip}^{q-1} \end{bmatrix}, \forall \alpha_i = \text{col}_{p=1}^{n}\{\alpha_{ip}\} \in \mathbb{R}^n. \tag{9}$$

Regarding the input with same features, then the *polynomial operator* becomes $\langle z_i, z_i \rangle = \text{col}_{p=1}^{n}\{\langle z_i, z_{ip} \rangle\}$ with

$$\langle z_i, z_{ip} \rangle = \begin{bmatrix} \sum_{q=1}^{d_j} z_{i1}^{d_j-q} z_{ip}^{q-1} \\ \sum_{q=1}^{d_j} z_{i2}^{d_j-q} z_{ip}^{q-1} \\ \vdots \\ \sum_{q=1}^{d_j} z_{ip}^{d_j-1} \\ \vdots \\ \sum_{q=1}^{d_j} z_{in}^{d_j-q} z_{ip}^{q-1} \end{bmatrix}, q \in \mathbb{Z}^+[1, d_j]. \tag{10}$$

It is worth pointing out that the pth element of $\langle z_i, z_{ip} \rangle$ is a polynomial of z_{ip} and the remaining elements are polynomials of z_{ig} and z_{ip} for $p, g \in \mathbb{Z}^+[1, n]$ and $g \neq p$. Let the augmented variables be $Z_i = [\langle z_i, a_i \rangle, \langle z_i, v_i \rangle, \langle z_i, z_i \rangle]^{\mathrm{T}}$ and $H_i^j = [\mathcal{M}_j, \mathcal{C}_j, \mathcal{K}_j]$, a more compact form of (8) can be derived by

$$y_i^j = H_i^j Z_i. \tag{11}$$

The polynomial coefficients in (11) for the jth rule can be estimated using the modified recursive least-square with dynamic forgetting factor (RLS-DFF):

$$\hat{H}_{i+1}^j = \hat{H}_i^j + \tilde{y}_{i+1}^j \frac{(P_i Z_{i+1})^{\mathrm{T}}}{\beta_{i+1} + (Z_{i+1})^{\mathrm{T}} P_i Z_{i+1}}, \tag{12}$$

$$P_{i+1} = \frac{1}{\beta_{i+1}} \left(P_i - \frac{P_i Z_{i+1} (Z_{i+1})^{\mathrm{T}} P_i}{\beta_{i+1} + (Z_{i+1})^{\mathrm{T}} P_i Z_{i+1}} \right), \tag{13}$$

$$\beta_{i+1} = \beta_0 + (1 - \beta_0) \left(1 - \tanh \left(\beta^* (\tilde{y}_{i+1}^j)^{\mathrm{T}} \tilde{y}_{i+1}^j \right) \right), \tag{14}$$

where $\tilde{y}_{i+1}^j = y_{i+1}^j - \hat{H}_i^j Z_{i+1}$ is the innovation vector. $\beta_i \in (0, 1]$ is the time-varying forgetting factor, which dynamically moderates the effect of new data on parameter estimates according to the innovation. $\beta_0 \in (0, 1]$ is a constant scalar initially defined for the forgetting factor. $\beta^* \in \mathbb{R}_+$ is a tuning parameter.

Considering the measurement noise in z_i and the system uncertainty, it is difficult to obtain the exact value of the associated membership grade, which is prone to enter the FOU formed by the upper and lower membership functions. In order to capture the uncertainty in the membership function, we model it as a Gaussian process with a squared exponential kernel function

$$\omega_j(z) \sim \mathcal{GP}(\mu_\omega(z), \kappa(z, z')) \tag{15}$$

where $\mu_\omega(z)$ and $\kappa(z, z')$ are the prior mean function (6) and the kernel function. Without loss of generality, each entry of the squared exponential kernel function is calculated as

$$[\kappa(z, z')]_{p\iota} = \sigma_\kappa^2 \exp \left(-\frac{\|z_p - z'_\iota\|^2}{2\eta_\kappa^2} \right) \tag{16}$$

where $z \in \mathbb{R}^{n \times N_z}$, $z' \in \mathbb{R}^{n \times N_{z'}}$, $p \in \mathbb{Z}^+[1, N_z]$ and $\iota \in \mathbb{Z}^+[1, N_{z'}]$. σ_κ and η_κ are the optimal hyperparameters obtained by maximizing marginal log-likelihood. Let $[z_\nu^*, \omega_j(z_\nu^*)]_{\nu=1}^m (m < N)$ be the random sample (observations) from the data set $[z_i, \omega_j(z_i)]_{i=1}^N$, the observations, therefore, follow a joint Gaussian distribution with the rest data (predictions)

$$\begin{bmatrix} \Omega_j^* \\ \omega_j(z_i) \end{bmatrix} \sim \mathcal{GP} \left(\begin{bmatrix} \mu_{\Omega_j^*} \\ \mu_\omega(z_i) \end{bmatrix}, \begin{bmatrix} \kappa(Z^*, Z^*) + \sigma_\epsilon^2 I & \kappa(Z^*, z_i) \\ \kappa(Z^*, z_i)^{\mathrm{T}} & \kappa(z_i, z_i) \end{bmatrix} \right), \tag{17}$$

in which $\Omega_j^* = \text{col}_{\nu=1}^m\{\omega_j(z_\nu^*)\}$, $Z^* = [z_1^*, z_2^*, \ldots, z_m^*]$, $i \neq \nu$. The observation noise considered in (17) is subject to the Gaussian distribution $\mathcal{N}(0, \sigma_\epsilon^2)$. Thus, the posterior membership function can be deduced according to marginalization and conditional distribution [29]

$$\omega_j(z_i) \sim \mathcal{GP} \left(\hat{\mu}_\omega(z_i), \sigma_\omega^2 \right) \tag{18}$$

where $\hat{\mu}_\omega(z_i) = \mu_\omega(z_i) + \kappa(Z^*, z_i)^{\mathrm{T}} (\kappa(Z^*, Z^*) + \sigma_\epsilon^2 I)^{-1} (\Omega_j^* - \mu_{\Omega_j^*})$ and $\sigma_\omega = (\kappa(z_i, z_i) - \kappa(Z^*, z_i)^{\mathrm{T}} (\kappa(Z^*, Z^*) + \sigma_\epsilon^2 I)^{-1} \kappa(Z^*, z_i))^{\frac{1}{2}}$. Let α be the confidence coefficient, the FOU induced by system uncertainty and measurement noise is limited by

$$\begin{aligned} \underline{\omega}_j(z_i) &= \hat{\mu}_\omega(z_i) - \alpha \sigma_\omega, \\ \bar{\omega}_j(z_i) &= \hat{\mu}_\omega(z_i) + \alpha \sigma_\omega, \end{aligned} \tag{19}$$

in which $\underline{\omega}_j(z_i)$ and $\bar{\omega}_j(z_i)$ denote the UMF and LMF for the corresponding rule such that $0 \leq \underline{\omega}_j(z_i) \leq \bar{\omega}_j(z_i) \leq 1$. In this regard, the firing strength of the rule j is within the following interval set:

$$W_j(z_i) = [\underline{\omega}_j(z_i), \bar{\omega}_j(z_i)], j \in \mathbb{Z}^+[1, l], \tag{20}$$

which leads to an interval set $[\underline{y}_i^j, \bar{y}_i^j]$, $j \in \mathbb{Z}^+[1, l]$ by substituting (20) into (7). The upper and lower bounds of y_i are processed in ascending order as $\{\underline{y}_i^{*j}\}$ and $\{\bar{y}_i^{*j}\}$, then the ordinal number of the associated membership function is adjusted to match the sorted output. The center-of-sets type-reduction method [30] is used to convert the interval set into crisp output:

$$\begin{aligned} y_{i\mathcal{L}} &= \min_{\xi \in \mathbb{Z}^+[1, l-1]} \frac{\sum_{*j=1}^{\xi} \bar{\omega}_{*j}(z_i) \underline{y}_i^{*j} + \sum_{*j=\xi+1}^{l} \underline{\omega}_{*j}(z_i) \underline{y}_i^{*j}}{\sum_{*j=1}^{\xi} \bar{\omega}_{*j}(z_i) + \sum_{*j=\xi+1}^{l} \underline{\omega}_{*j}(z_i)} \\ &= \frac{\sum_{*j=1}^{L} \bar{\omega}_{*j}(z_i) \underline{y}_i^{*j} + \sum_{*j=L+1}^{l} \underline{\omega}_{*j}(z_i) \underline{y}_i^{*j}}{\sum_{*j=1}^{L} \bar{\omega}_{*j}(z_i) + \sum_{*j=L+1}^{l} \underline{\omega}_{*j}(z_i)}, \end{aligned} \tag{21}$$

$$\begin{aligned} y_{i\mathcal{R}} &= \max_{\xi \in \mathbb{Z}^+[1, l-1]} \frac{\sum_{*j=1}^{\xi} \underline{\omega}_{*j}(z_i) \bar{y}_i^{*j} + \sum_{*j=\xi+1}^{l} \bar{\omega}_{*j}(z_i) \bar{y}_i^{*j}}{\sum_{*j=1}^{\xi} \underline{\omega}_{*j}(z_i) + \sum_{*j=\xi+1}^{l} \bar{\omega}_{*j}(z_i)} \\ &= \frac{\sum_{*j=1}^{R} \underline{\omega}_{*j}(z_i) \bar{y}_i^{*j} + \sum_{*j=R+1}^{l} \bar{\omega}_{*j}(z_i) \bar{y}_i^{*j}}{\sum_{*j=1}^{R} \underline{\omega}_{*j}(z_i) + \sum_{*j=R+1}^{l} \bar{\omega}_{*j}(z_i)}, \end{aligned} \tag{22}$$

where L and R are the switching points obtained by Karnik–Mendel (KM) or EKM algorithm [31], [32] such that

$\underline{y}_i^L \leq y_{i\mathcal{L}} \leq \underline{y}_i^{L+1}$ and $\bar{y}_i^R \leq y_{i\mathcal{R}} \leq \bar{y}_i^{R+1}$. Hence, the crisp output of the IT2 PFMB system can be calculated as:

$$y_i = \frac{y_{i\mathcal{L}} + y_{i\mathcal{R}}}{2}, \tag{23}$$

which therefore completes the entire modeling procedure that is summarized in the *Algorithm* 1.

Algorithm 1: Data-Driven GP-IT2PFL Algorithm

Data: Input-Output pair data $[x_i, y_i]_{i=1}^N$
Result: IT2 polynomial fuzzy system and identified clusters

```
Z-Score normalization for the collected x_i
Calculate the cluster centres and prior membership functions as (5) and (6)
while i ≤ N do
    Conduct state augmentation as Z_i using polynomial operator
    Update the parameter matrices as (12)-(14)
    Construct the Gaussian process for membership function as (15)
    Calculate the UMF and LMF as (19)
    Calculate the IT2 polynomial fuzzy output as (23)
end
```

Remark 3: The first and second-order derivatives of the input data are also included in the observation matrix (8), where the adopted UKF technique facilitates noise attenuation. Additionally, the implementation of z-score normalization as described in (1) assists in mitigating the detrimental impact of input noise on the clustering outcomes. Therefore, it facilitates the expression of the two-limb coordination trajectories. It ensures that the *polynomial-operator-based* modeling approach is more effective to extract the nonlinear features of MIMO mapping, compared to traditional methods that treat the input data as independent [25], [33]–[35].

Remark 4: In contrast to [35], [36] which consider parameter corrections to build IT2 fuzzy sets, a non-parametric Gaussian process is utilised to model uncertainty in the membership function directly. The resulting FOU benefits from capturing the parameter perturbations and the black-box characteristics due to measurement noise and system uncertainty. It is worth noting that the membership function in (6) is utilized as the prior mean function $\mu_\omega(z_i)$ when reconstructing the FOU in terms of uncertainty. The inverse of the covariance matrix $(\kappa(Z^*, Z^*) + \sigma_\epsilon^2 I)$ can be effectively numerically calculated through Cholesky decomposition.

III. Coordinated Manipulation

We have carried out two experiments to check whether the proposed algorithm can capture coordination patterns between human limbs. In this section, we first test the hand-foot coordination of a solo operator in three bimanual picking and placing tasks.

A. Experiments

This experiment was conducted at the Institute of Perception, Action, and Behaviour at Edinburgh University. The bimanual hand-foot coordination system is composed of two torque-controlled, 7-DoF Franka Emika robotic manipulators, which are both equipped with a flat 3D-printed contact plate mounted on the end-effector. The bimanual impedance controller [37] is implemented in velocity and offset modes to make full use of the robot workspace while ensuring safe interaction with the environment. Real-time module calculation is performed on the basis of the rigid-body dynamic library *Pinocchio*, where *EiQuadProg++* is used to solve quadratic programs for inverse kinematics. The operator can provide 6-DoF (position and orientation) commands via the foot interface and Sigma-7 haptic device (Force Dimension Inc., Switzerland), where the foot interface is a parallel-serial-structure [38] using multiple force sensors to collect the foot position and force information in four DoFs. The gravity compensations for both hand and foot interfaces are set to assist human manipulation and eliminate human fatigue.

We carry out three typical tasks based on the hand-foot coordination system, namely (1) picking and placing a deformable object (Fig. 2a-c); (2) picking and placing a rigid block (Fig. 2d-f); and (3) grasping a mobile object on the treadmill (Fig. 2g-i). The object block in tasks 2 and 3 has a rectangular shape ($12 \times 16 \times 14\,\mathrm{cm}$), weight $0.8\,\mathrm{kg}$, and is fitted with interconnecting industrial fittings (Anderson Power Mid-Power Spec-Pak). Task 1 involves capturing the softball located above the block and then moving it to the basin in the red area. Notice that the block is removed after the grasping action is completed to avoid collisions. In task 2, the block located in the red area on the right side is first transferred to the red area on the left side and then placed back in its original position on the right side. With respect to task 3, the dual-arm robot's objective is to grab the block moving on the treadmill and place it in the red rectangle. The three tasks are progressively more difficult and require higher levels of hand-foot coordination, ranging from static to dynamic grasping.

At the training stage, the aforementioned three tasks are performed by the left hand and foot corresponding to the left and right robotic manipulators, respectively, whose spatial motion positions on the x, y, and z axis are fed into the proposed approach as inputs. Subsequently, the left manipulator moves according to the commands generated by the proposed algorithm at the test stage, while the right robot arm is controlled by the foot interface. The parameters are set as $l = 4$, $\chi = 2$, $\alpha = 1.96$, $N = 1000$, $\sigma_\epsilon = 0.1$, $\sigma_\kappa = 0.6009$, $\eta_\kappa = 0.0053$, and $\Delta T = 0.01$s.

B. Results

To examine the performance of the GP-IT2PFL approach, we evaluate the estimation performance by root-mean-square error:

$$\mathrm{RMSE} = \sqrt{\frac{1}{N}\sum_{i=1}^{N} \|y_i - \hat{y}_i\|^2}, \tag{24}$$

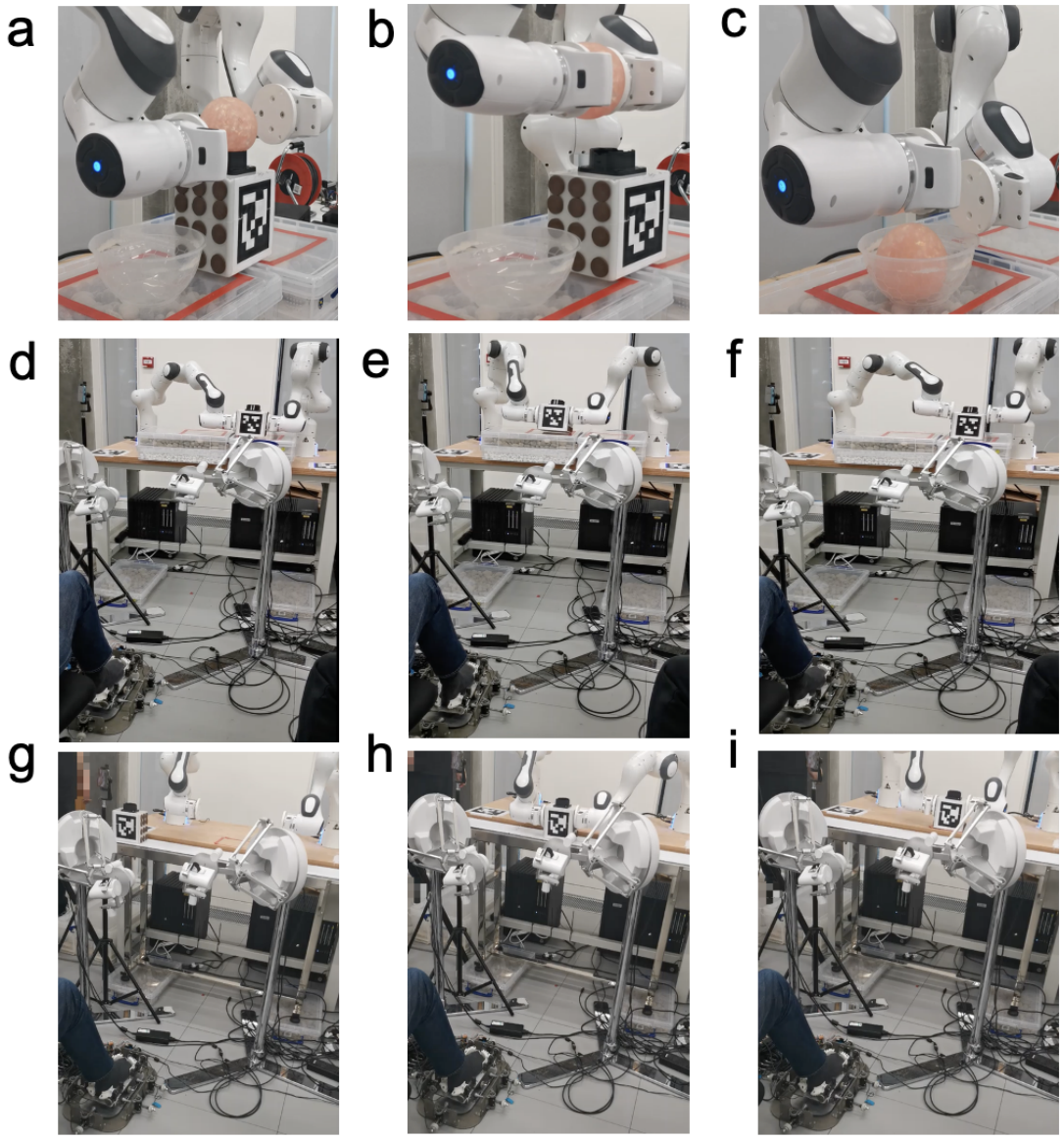

Fig. 2. Hand-foot coordinated manipulation tasks. Side views of the (a) initial, (b) grasping, and (c) placing stages of task 1; Demonstration in the operator views of the initial grasping (d), intermediate positioning (e), and final placing (f) stages in task 2; Demonstration in the operator views of the initial (g), grasping (h), and placing (i) stages of task 3.

where y_i and $\hat{y}_i$ represent the actual and the estimated end-effector position, respectively. We construct the neural network [39] and Gaussian process [40] for three tasks in bimanual hand-foot coordination for comparison, where the dataset is identical with the GP-IT2PFL approach, and the number of samples is 5000 (training: 4000, test: 1000) based on an empirical ratio in [41]. In particular, the neural network (NN) is composed of 2 hidden layers with 40 and 20 neurons with hyperbolic tangent and rectified linear unit (ReLU) activation functions, the final output layer is with log-sigmoid activation function, where the parameters of the NN are initialized by [42]. Table I presents the comparative results in tasks 1-3, where each value represents the average of the x, y, and z-axis trajectory estimation errors corresponding to different methods. The estimated membership functions subject to UMF and LMF are depicted in Fig. 3, where the practical membership functions subject to measurement errors and uncertainties are effectively captured by the UMF and LMF. We see that the proposed algorithm enables the human to perform bimanual tasks only by foot interface independent of the intervention of two hands.

TABLE I
THE AVERAGE RMSES OF x, y, AND z-AXIS TRAJECTORIES FOR HAND-FOOT COORDINATED MANIPULATION.

Task	Neural Network	GP	**GP-IT2PFL**
Task 1	0.5808	0.5824	**0.074**
Task 2	0.2337	0.2254	**0.053**
Task 3	0.5511	0.5556	**0.023**

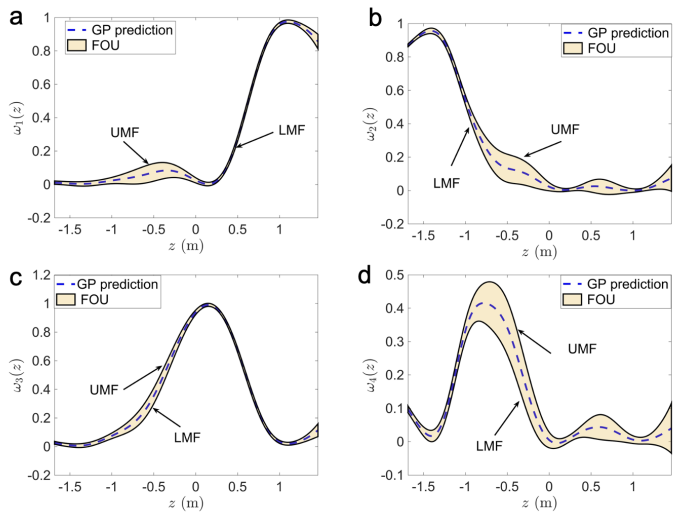

Fig. 3. IT2 membership functions developed through Gaussian process (18) in task 1 of hand-foot coordination manipulation. (a)-(d) illustrate the membership grade predictions corresponding to $\mathcal{B}_1$, $\mathcal{B}_2$, $\mathcal{B}_3$ and $\mathcal{B}_4$, respectively. The solid black lines between the yellow area represent the UMF and LMF, respectively.

IV. Shared Telesurgery

To further assess the performance of the proposed method, we carried out a second experiment on human-human bimanual surgical manipulation using the Da Vinci surgical robotic system at Imperial's Hamlyn Center for Robotic Surgery.

A. Experiments

The experimental setup is shown in Fig. 4. The local console (Fig. 4a) consists of two Omega-7 haptic interfaces (Force Dimension Inc., Switzerland) and a monitor providing visual feedback of the patient side. We assume that the operator can execute the task using top-down visual feedback as in typical Laparoscopy. Two patient-side manipulators (PSM) of Da Vinci robotic system (Intuitive Surgical, USA) are used as remote robotic arms as shown in Fig. 4b. Regulated by the Omega-7 controller, the hand-driven handle motion is directly mapped to three-dimensional translations and one roll rotation of PSM's end-effector.

The standard training task peg transfer from Fundamentals of Laparoscopic Surgery (FLS) [43] is selected as the testing task for human-robot collaboration. This task can simulate the surgical scenario that transfers the detached gallstones to the collection tool from the primary surgeon to the assistant. In our case, the human assistant is replaced by an automatic robotic partner to facilitate the surgeon to complete the task. The training data was collected from human-human collaboration and was tested in human-robot collaboration.

We collect the trajectory data from the Omega-7 end-effector in human-human cooperation. As shown in Fig. 5a, the PSM gripper follows the commands from the end-effector of the local interface, where the left PSM gripper is controlled by the main operator and the right one by an assistant. The main operator navigates the left gripper onto the initial peg, grabs the orange block, lifts it, and moves it to the assistant-controlled gripper on the right for the handover. Then, the right-hand gripper moves the block to the target peg and finally releases it (see supplementary video 1), as demonstrated in Fig. 5b. The manipulation data of the main operator (left gripper), including spatial motion positions on x, y, z axis and the open angle of the gripper θ, are fed as inputs of the proposed algorithm, while the assistive operator (right gripper) motion data are the outputs. As the surgical robot system lacks force/torque sensors, we have used the open angle of the gripper to correspond to the grasping force.

B. Results

Fig. 6a shows the real right-hand trajectories and the estimation ones in human-human cooperation, where the assistive operator movement is effectively represented with minimal error. The RMSEs of the estimation errors in x, y and z directions are 4.2036×10^{-4}m, 5.3761×10^{-4}m and 5.3254×10^{-4}m, respectively. Similarly, Fig. 6b depicts the estimation profiles of right-hand gripper trajectories in human-human cooperation. The main operator moves the left-hand gripper to the initial peg at the beginning. Upon arrival, the left-hand gripper opens and grasps the block in 8.3s, then transfers the block to the right-hand gripper, as shown in Fig. 6b. It can be found that the right-hand gripper increases its opening angle to take over the object within 7.47s. The estimated angle of the right-hand gripper is close to the real angle in terms of time duration (0.93s difference) and degree (RMSE = 0.7571°). The opening angle of the right-hand gripper and left-hand gripper in Fig. 6 are respectively denoted by positive and negative values of θ.

Four trained mappings (three for translations and one for gripper angle) are implemented for the right-hand robotic manipulator of the surgical robotic system. It acts as an assistive robot cooperating with the human operator according to the operator's real-time manipulation. Figs. 6c-d demonstrate the trained assistive robot motion at the test stage (human-robot collaboration), which recognizes human motion and cooperates accordingly. For example, the assistive robot gripper waits for the operator's action within an initial period of 2.93s. When the assistive robot recognizes that the main operator has grasped the object and is moving toward it, it adjusts the opening angle of the gripper to hand over the object, which takes approximately 19.11s. After the object is successfully transferred and the human operator releases the grasping, the assistive robot holds the object and quickly moves to the target peg in 21.37s (see supplementary video 2). With the involvement of the assistive robot, the main operator completes the entire task in 27s.

V. Discussion

This paper proposed a new GP-IT2PFL framework to facilitate robot motion learning with tailored assistance in human-robot cooperation, which enables humans to perform bimanual tasks with one limb. This algorithm solved the coupling issue between intra- and inter-input data in two-limb coordination using the polynomial operator and minimized

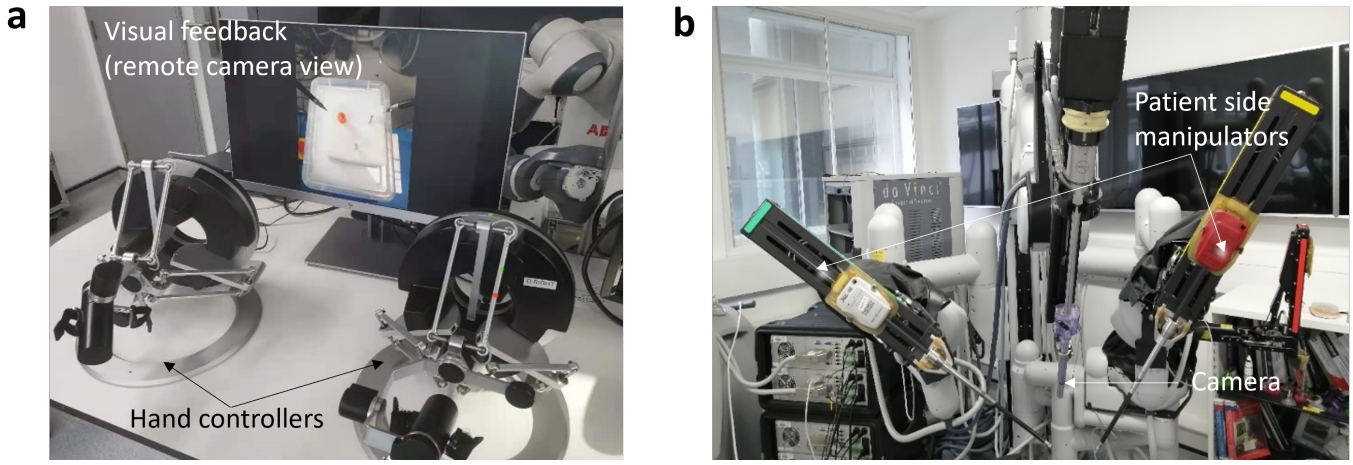

Fig. 4. Experimental setup for robotic surgery: Da Vinci system for laparoscopic surgery with Omega-7 hand controllers. (a) The local console includes dual Omega-7 hand controllers and one monitor to provide visual feedback from the remote side. (b) Da Vinci surgical robotic system with dual manipulators and one camera at the remote side.

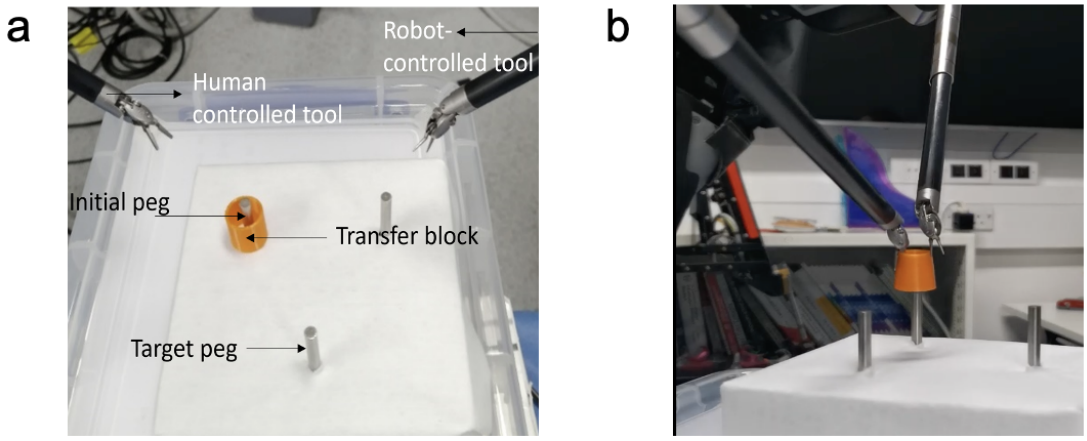

Fig. 5. Cooperative peg-transfer task. (a) The human operator controls the left side tool to grasp the block object on the initial peg and passes it to the robot-controlled tool. (b) The robot-controlled tool takes over the transfer block and moves it to the target peg.

the system uncertainty and measurement noise by Gaussian-process-based upper and lower membership functions. The proposed approach was tested in two applications: solo two-limb coordination and dyad collaboration. The successful implementation requires the same subject to perform a consistent and stable motion strategy under the same initial conditions during training and test phases, where the parameters in the associated fuzzy model are tailored to this subject.

Fig. 3 demonstrates that the system uncertainty can be captured by the FOU that is constructed by UMF and LMF. It indicates that any system whose membership functions are within the GP-based FOU can be represented by the GP-IT2PFL approach. Different from traditional T-S fuzzy algorithms [33], [34], [41], system uncertainty and measurement noise can be handled simultaneously by GP-based UMF and LMF. Therefore, the GP-IT2PFL algorithm can represent a wider range of multiple-limb coordination behaviors compared with existing approaches.

As shown in Fig. 3, the estimation output is regarded as a weighted sum of four polynomial models, whose weights are embodied by the data-driven membership function (6). In addition, since the intrinsic coupling effects between intra- and inter-input data of x, y, and z-axis trajectories are effectively represented by the polynomial operator, the GP-IT2PFL algorithm shows the highest fitting accuracy in Table I.

The experimental results on manipulation with hand-foot control demonstrate the potential of the proposed method for multi-limb coordination tasks. Foot interfaces can free the operator's hands and enable them carrying out tasks with three or four instruments using both their hands and feet. Using a similar approach, recent studies showed promising results of using the feet to control an industrial robot [44], [45]. We have verified that movements controlled by a foot in coordination with one hand can be learned to develop an autonomous behavior or augment one-hand control of a robot, which is a first step towards using coordinated movements learned with our method. These results indicate that we can now explore a similar approach for enhancing the movements of both hands, towards enabling an operator to perform tri- or quad-manipulation by the hands, with some robot arms controlled

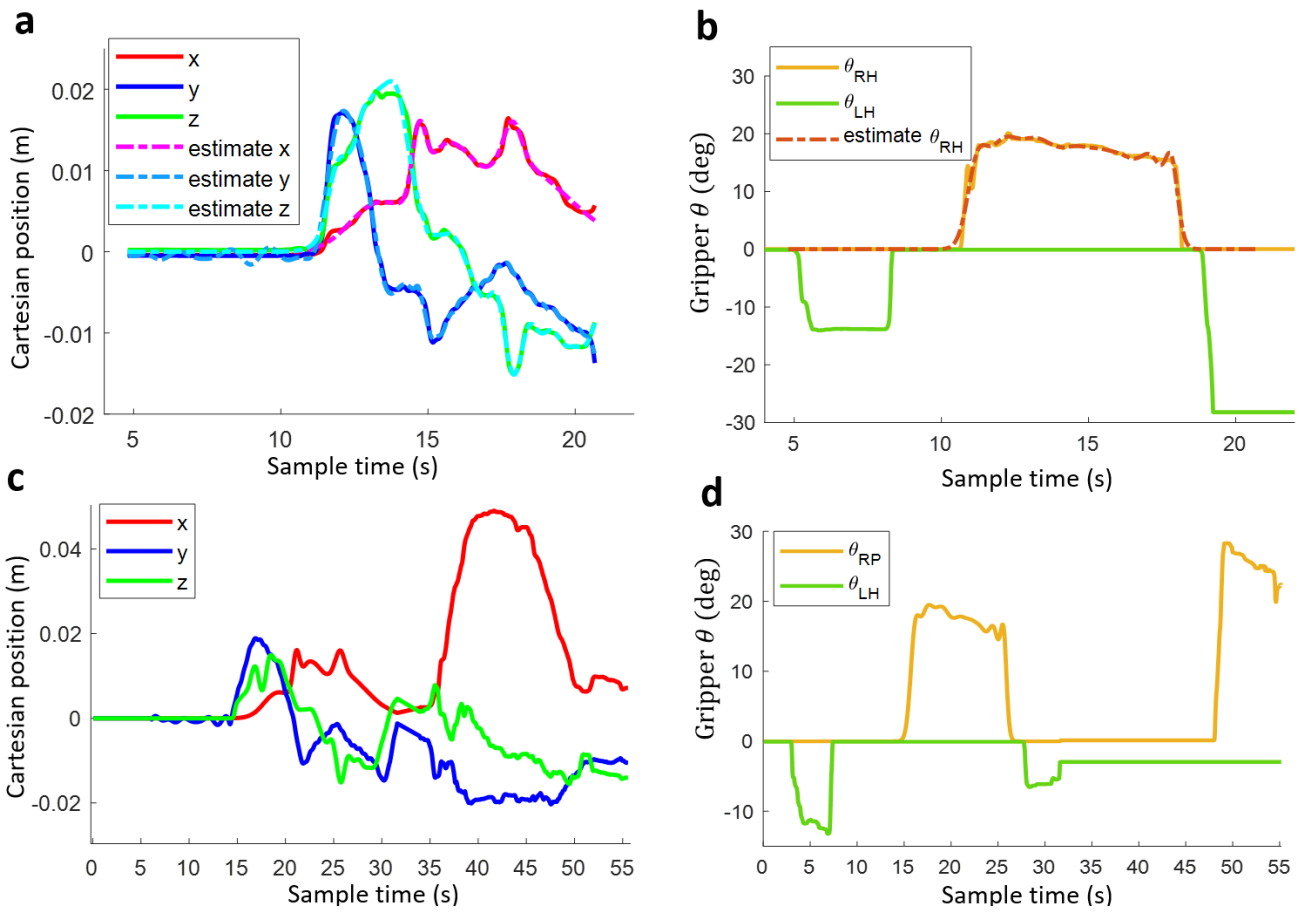

Fig. 6. Experimental results from (a-b) human-human training to (c-d) human-robot test. Trajectory learning from the main operator and assistive operator: (a) Cartesian trajectories in human-human telesurgery (x, y and z denote the right-hand movement along the associated direction. The dashed lines are the estimate with respect to the associated direction using the proposed method). (b) Gripper grasping θ: the dashed line stands for the estimate of gripper movement. θ_{LH} and θ_{RH} represent the angle at which the left and right-hand grippers open. Trajectory learning from the human operator and assistive robot: (c) Cartesian trajectories in human-robot telesurgery (x, y, and z denote the assistive robot movement along the associated direction). (d) Assistive gripper grasping: θ_{RP} is the angle of the assistive robot gripper.

directly with the hands and the other through coordinated motion learned from previous interactions.

Fig. 6 shows that similar behaviors are generated with the GP-IT2PFL algorithm (Fig. 6 c,d), compared with the trajectories and gripper movement of the assistive operator (Fig. 6 a,b). Furthermore, the experiment results on the Da Vinci surgical system have shown that the assistive robot can reduce the intensity of the surgeon's manipulation effectively by implementing the proposed method, which facilitates assisting and adapting to surgeon behavior autonomously. Trained by the trajectories and gripper movements of human-human collaboration, intuitive human-robot cooperation was demonstrated in a peg-transfer task with self-determining movements from the assistive robot.

With the assistive robot, the surgeon can perform the peg-transfer task alone thus avoiding potential communication errors with an assistant. Moreover, Fig. 6 demonstrates that the proposed GP-IT2PFL approach allows for modeling the coordinated gripper movements. Hence, the assistive robot driven by the proposed method embodies the capability to assist humans with telesurgery tasks in the force-sensor-free scenario. It sheds light on the fact that the proposed algorithm is effective in modeling human motion adaptation.

References

[1] M. Wonsick, P. Long, A. Ö. Önol, M. Wang, and T. Padır, "A holistic approach to human-supervised humanoid robot operations in extreme environments," *Frontiers in Robotics and AI*, vol. 8, p. 148, 2021.

[2] D. Huang, B. Li, Y. Li, and C. Yang, "Cooperative manipulation of deformable objects by single-leader–dual-follower teleoperation," *IEEE Transactions on Industrial Electronics*, vol. 69, no. 12, pp. 13 162–13 170, 2022.

[3] N. Tahir and R. Parasuraman, "Analog twin framework for human and ai supervisory control and teleoperation of robots," *IEEE Transactions on Systems, Man, and Cybernetics: Systems*, pp. 1–13, 2022.

[4] Z. Huang, Z. Wang, W. Bai, Y. Huang, L. Sun, B. Xiao, and E. M. Yeatman, "A novel training and collaboration integrated framework for human–agent teleoperation," *Sensors*, vol. 21, no. 24, p. 8341, 2021.

[5] A. Takagi, G. Ganesh, T. Yoshioka, M. Kawato, and E. Burdet, "Physically interacting individuals estimate the partner's goal to enhance their movements," *Nature Human Behaviour*, vol. 1, pp. 1–6, 2017.

[6] G. Carboni, T. Nanayakkara, A. Takagi, and E. Burdet, "Adapting the visuo-haptic perception through muscle coactivation," *Scientific Reports*, vol. 11, no. 1, pp. 1–7, 2021.

[7] Y. Li, A. Sena, Z. Wang, X. Xing, J. Babic, E. H. van Asseldonk, and E. Burdet, "A review on interaction control for contact robots through intent detection," *Progress in Biomedical Engineering*, vol. 4, no. 3, p. 032004, 2022.

[8] J. Tobin, R. Fong, A. Ray, J. Schneider, W. Zaremba, and P. Abbeel, "Domain randomization for transferring deep neural networks from simulation to the real world," in *IEEE/RSJ International Conference on Intelligent Robots and Systems (IROS)*, 2017, pp. 23–30.

[9] W. Zhao, J. P. Queralta, and T. Westerlund, "Sim-to-real transfer in deep reinforcement learning for robotics: a survey," in *IEEE Symposium Series on Computational Intelligence (SSCI)*, 2020, pp. 737–744.

[10] J. Zhong, J. Li, A. Lotfi, P. Liang, and C. Yang, "An incremental cross-modal transfer learning method for gesture interaction," *Robotics and Autonomous Systems*, vol. 155, p. 104181, 2022.

[11] J. Ibarz, J. Tan, C. Finn, M. Kalakrishnan, P. Pastor, and S. Levine, "How to train your robot with deep reinforcement learning: lessons we have learned," *The International Journal of Robotics Research*, vol. 40, no. 4-5, pp. 698–721, 2021.

[12] I. Havoutis and S. Calinon, "Learning from demonstration for semi-autonomous teleoperation," *Autonomous Robots*, vol. 43, no. 3, pp. 713–726, 2019.

[13] Z. Chen, Z. Wang, R. Liang, B. Liang, and T. Zhang, "Virtual-joint based motion similarity criteria for human–robot kinematics mapping," *Robotics and Autonomous Systems*, vol. 125, p. 103412, 2020.

[14] G. Katz, D.-W. Huang, T. Hauge, R. Gentili, and J. Reggia, "A novel parsimonious cause-effect reasoning algorithm for robot imitation and plan recognition," *IEEE Transactions on Cognitive and Developmental Systems*, vol. 10, no. 2, pp. 177–193, 2017.

[15] L. Vianello, J.-B. Mouret, E. Dalin, A. Aubry, and S. Ivaldi, "Human posture prediction during physical human-robot interaction," *IEEE Robotics and Automation Letters*, vol. 6, no. 3, pp. 6046–6053, 2021.

[16] C. Meo, G. Franzese, C. Pezzato, M. Spahn, and P. Lanillos, "Adaptation through prediction: Multisensory active inference torque control," *IEEE Transactions on Cognitive and Developmental Systems*, vol. 15, no. 1, pp. 32–41, 2023.

[17] S. C. Bacha, W. Bai, Z. Wang, B. Xiao, and E. M. Yeatman, "Deep reinforcement learning-based control framework for multilateral telesurgery," *IEEE Transactions on Medical Robotics and Bionics*, vol. 4, no. 2, pp. 352–355, 2022.

[18] J. Luo, D. Huang, Y. Li, and C. Yang, "Trajectory online adaption based on human motion prediction for teleoperation," *IEEE Transactions on Automation Science and Engineering*, vol. 19, no. 4, pp. 3184–3191, 2022.

[19] H.-K. Lam, "A review on stability analysis of continuous-time fuzzy-model-based control systems: From membership-function-independent to membership-function-dependent analysis," *Engineering Applications of Artificial Intelligence*, vol. 67, pp. 390–408, 2018.

[20] T. Takagi and M. Sugeno, "Fuzzy identification of systems and its applications to modeling and control," *IEEE Transactions on Systems, Man, and Cybernetics*, vol. SMC-15, no. 1, pp. 116–132, 1985.

[21] H.-K. Lam, *Polynomial Fuzzy Model-Based Control Systems: Stability Analysis and Control Synthesis Using Membership Function Dependent Techniques*. Springer, 2016.

[22] J. Li, C. Hua, Y. Yang, and X. Guan, "Bayesian block structure sparse based T–S fuzzy modeling for dynamic prediction of hot metal silicon content in the blast furnace," *IEEE Transactions on Industrial Electronics*, vol. 65, no. 6, pp. 4933–4942, 2018.

[23] M. Luo, F. Sun, and H. Liu, "Joint block structure sparse representation for Multi-Input–Multi-Output (MIMO) T–S fuzzy system identification," *IEEE Transactions on Fuzzy Systems*, vol. 22, no. 6, pp. 1387–1400, 2014.

[24] W. Zou, C. Li, and N. Zhang, "A T–S fuzzy model identification approach based on a modified inter type-2 frcm algorithm," *IEEE Transactions on Fuzzy Systems*, vol. 26, no. 3, pp. 1104–1113, 2018.

[25] E.-H. Kim, S.-K. Oh, and W. Pedrycz, "Design of reinforced interval type-2 fuzzy c-means-based fuzzy classifier," *IEEE Transactions on Fuzzy Systems*, vol. 26, no. 5, pp. 3054–3068, 2018.

[26] B.-I. Choi and F. C.-H. Rhee, "Interval type-2 fuzzy membership function generation methods for pattern recognition," *Information Sciences*, vol. 179, no. 13, pp. 2102–2122, 2009.

[27] J. C. Bezdek, *Pattern Recognition with Fuzzy Objective Function Algorithms*. Springer Science & Business Media, 2013.

[28] S. L. Chiu, "Fuzzy model identification based on cluster estimation," *Journal of Intelligent & Fuzzy Systems*, vol. 2, no. 3, pp. 267–278, 1994.

[29] C. K. Williams and C. E. Rasmussen, *Gaussian Processes for Machine Learning*. MIT Press, 2006.

[30] J. M. Mendel, *Uncertain Rule-Based Fuzzy Systems: Introduction and New Directions (Second Edition)*. Springer, 2017.

[31] N. Karnik, J. Mendel, and Q. Liang, "Type-2 fuzzy logic systems," *IEEE Transactions on Fuzzy Systems*, vol. 7, no. 6, pp. 643–658, 1999.

[32] D. Wu and J. M. Mendel, "Enhanced karnik–mendel algorithms," *IEEE Transactions on Fuzzy Systems*, vol. 17, no. 4, pp. 923–934, 2009.

[33] J. Dai, H. Lam, and S. Vahed, "Soil type identification for autonomous excavation based on dissipation energy," *Proceedings of the Institution of Mechanical Engineers, Part I: Journal of Systems and Control Engineering*, vol. 225, no. 1, pp. 35–50, 2011.

[34] S. Wen, H. Yu, B. Zhang, Y. Zhao, H.-K. Lam, G. Qin, and H. Wang, "Fuzzy identification and delay compensation based on the force/position control scheme of the 5-dof redundantly actuated parallel robot," *International Journal of Fuzzy Systems*, vol. 19, no. 1, pp. 124–140, 2017.

[35] S.-H. Tsai and Y.-W. Chen, "A novel interval type-2 fuzzy system identification method based on the modified fuzzy c-regression model," *IEEE Transactions on Cybernetics*, pp. 1–12, 2021.

[36] D. Wu and W. Tan, "A type-2 fuzzy logic controller for the liquid-level process," in *IEEE International Conference on Fuzzy Systems*, vol. 2, 2004, pp. 953–958.

[37] A. Sena, Q. Rouxel, E. Ivanova, E. Burdet, and Z. Li, "Haptic bimanual system for teleoperation of time-delayed tasks," in *2021 IEEE International Conference on Robotics and Biomimetics (ROBIO)*. IEEE, 2021, pp. 1234–1239.

[38] Y. Huang, E. Burdet, L. Cao, P. T. Phan, A. H. T. Meng, and L. Phee, "A subject-specific four-degree-of-freedom foot interface to control a surgical robot," *IEEE/ASME Transactions on Mechatronics*, vol. 25, no. 2, pp. 951–963, 2020.

[39] G. Papageorgiou, P. Bouboulis, and S. Theodoridis, "Robust linear regression analysis-a greedy approach," *IEEE Transactions on Signal Processing*, vol. 63, no. 15, pp. 3872–3887, 2015.

[40] C. K. I. Williams and C. E. Rasmussen, *Gaussian Processes for Machine Learning*, ser. Adaptive Computation and Machine Learning series. MIT Press, 2019.

[41] G. Jia, H.-K. Lam, S. Ma, Z. Yang, Y. Xu, and B. Xiao, "Classification of electromyographic hand gesture signals using modified fuzzy c-means clustering and two-step machine learning approach," *IEEE Transactions on Neural Systems and Rehabilitation Engineering*, vol. 28, no. 6, pp. 1428–1435, 2020.

[42] K. He, X. Zhang, S. Ren, and J. Sun, "Delving deep into rectifiers: Surpassing human-level performance on imagenet classification," in *IEEE International Conference on Computer Vision*, 2015, pp. 1026–1034.

[43] H.-C. Hur, D. Arden, L. E. Dodge, B. Zheng, and H. A. Ricciotti, "Fundamentals of laparoscopic surgery: A surgical skills assessment tool in gynecology," *JSLS Journal of the Society of Laparoscopic & Robotic Surgeons*, vol. 15, no. 1, pp. 21–26, 2011.

[44] M. Y. Saraiji, T. Sasaki, K. Kunze, K. Minamizawa, and M. Inami, "Metaarms: Body remapping using feet-controlled artificial arms," in *Proceedings of the 31st Annual ACM Symposium on User Interface Software and Technology*, 2018, pp. 65–74.

[45] W. Amanhoud, J. Hernandez Sanchez, M. Bouri, and A. Billard, "Contact-initiated shared control strategies for four-arm supernumerary manipulation with foot interfaces," *The International Journal of Robotics Research*, vol. 40, no. 8-9, pp. 986–1014, 2021.